Nanoscale $LiFePO_4$ and $Li_4Ti_5O_{12}$ for High Rate Li-ion Batteries

A. Jaiswal[1], C. R. Horne[1], O. Chang[1], W. Zhang[1], W. Kong[1], E. Wang[2], T. Chern,[2] and M. M. Doeff[2]

[1]NanoGram Corporation, 165 Topaz St. Milpitas CA 95035

[2]Materials Science Division

Lawrence Berkeley National Laboratory, University of California, Berkeley

CA 94720

Keywords: $LiFePO_4$, $Li_4Ti_5O_{12}$, Nanomaterial, Li-ion Battery

Corresponding Author: A. Jaiswal (ajaiswal@nanogram.com)

Abstract

The electrochemical performances of nanoscale $LiFePO_4$ and $Li_4Ti_5O_{12}$ materials are described in this communication. The nanomaterials were synthesized by pyrolysis of an aerosol precursor. Both compositions required moderate heat-treatment to become electrochemically active. $LiFePO_4$ nanoparticles were coated with a uniform, 2-4 nm thick carbon-coating using an organic precursor in the heat treatment step and showed high tap density of 1.24 g/cm^3, in spite of 50-100 nm particle size and 2.9 wt% carbon content. $Li_4Ti_5O_{12}$ nanoparticles were between 50-200 nm in size and showed tap density of 0.8 g/cm^3. The nanomaterials were tested both in half cell configurations against Li-metal and also in $LiFePO_4/Li_4Ti_5O_{12}$ full cells. Nano-$LiFePO_4$ showed high discharge rate capability with values of 150 and 138 mAh/g at C/25 and 5C, respectively, after constant C/25 charges. Nano-$Li_4Ti_5O_{12}$ also showed high charge capability with values of 148 and 138 mAh/g at C/25 and 5C, respectively, after constant C/25 discharges; the discharge (lithiation) capability was comparatively slower. $LiFePO_4/Li_4Ti_5O_{12}$ full cells deliver charge/discharge capacity values of 150 and 122 mAh/g at C/5 and 5C, respectively.

Introduction

The next generation of Li-ion batteries for consumer electronics and for automobile applications (electric vehicles (EVs) and hybrid electric vehicles (HEVs)) have to provide benefits of cost, safety, rate capability, and environmental compatibility. In this regard, $LiFePO_4$ and $Li_4Ti_5O_{12}$ are promising active materials for positive and negative electrodes, respectively.[1-4] $LiFePO_4$ shows a specific capacity of 170 mAh/g with a flat discharge-charge profile at 3.4 V vs. Li, which makes it compatible with most commonly used electrolytic solutions.[1-2] $Li_4Ti_5O_{12}$ is a zero strain material (no volume change on lithiation/delithiation) with a flat discharge-charge profile at 1.55 V vs. Li and a specific capacity of 175 mAh/g.[3-4] However for practical applications, both compositions are limited by their inherent low electronic conductivity. Several different approaches have been proposed to overcome this barrier. One is particle size reduction into the nano-regime, resulting in shorter diffusion distances; a second is carbon coating $LiFePO_4$ particles to enhance surface electronic conductivity; and a third controversial one is doping with aliovalent cations to enhance the bipolar conductivity of $LiFePO_4$ particles.[5-7] $Li_4Ti_5O_{12}$ is a poor electronic conductor which on lithiation shows good electronic conductivity on the particle surface due to presence of mixed Ti^{4+}/Ti^{3+} valence; during delithiation the reversal is expected which would result in poor electronic conductivity on particle surface. To improve rate performance of $Li_4Ti_5O_{12}$, doping with aliovalent cations to improve bulk electronic conductivity and particle size reduction to reduce diffusion distance has been suggested.[8-10] In this paper, we explore the particle size reduction route for $LiFePO_4$ and $Li_4Ti_5O_{12}$ compositions, along with carbon-coating of the $LiFePO_4$ particles to increase the electronic conductivity.

Experimental

Synthesis of the $LiFePO_4$ and $Li_4Ti_5O_{12}$ nanoparticles was done by conversion of an aerosol precursor using a proprietary pyrolysis technique. A liquid precursor, containing elemental compounds in the desired stoichiometric ratios, was atomized into fine droplets and introduced into the reaction zone leading to a localized pyrolysis reaction and formation of nanoparticles with homogenous composition. A rapid quenching of particles limits the size growth. The synthesized nanoparticles are then entrained in the used process gas stream and collected in a filter-housing. A moderate heat-treatment step was required to achieve electrochemically active, nanostructured materials; the heat-treatment was done in an inert/reducing atmosphere for $LiFePO_4$ material and in air for $Li_4Ti_5O_{12}$. $LiFePO_4$ nanoparticles were coated with carbon in the heat-treatment step using an organic precursor. Post synthesis the powders were handled and stored under ambient conditions.

X-ray diffraction (XRD) powder patterns of materials were collected using a Rigaku Miniflex diffractometer and analyzed using JADE software (MDI). The particles were analyzed using scanning electron microscopy (SEM, Hitachi S-4100) and transmission electron microscopy (TEM, JEOL JEM-2010). Brunauer-Emmett-Teller (BET) specific surface areas were measured using a Micromeritics TriStar 3000 gas absorption analyzer. Tap-densities and pellet-densities of the samples were measured using in-house built equipment. Fourier Transform infrared (FTIR) and Raman spectra were collected using a Perkin Elmer-Spectrum 2000 and an integrated confocal Raman microscope system, "Labram," made by ISA Group Horiba, as previously described,[11]

respectively. The carbon content of the samples was analyzed using combustion infrared detection according to ASTM E 1019-03.

Electrodes were composed of 80 wt% active material, 8 wt% Kynar poly(vinylidene fluoride) (PVDF) (Elf Atochem North America Inc., Technical Polymers Department), 6 wt% SFG-6 synthetic flake graphite (Timcal Ltd., Graphites and Technologies), and 6 wt% acetylene black. Slurries of the mixture in 1-methyl-2-pyrrolidinone (Sigma Aldrich, 99%) were cast onto carbon coated aluminum current collectors (Intelicoat Technologies) and dried for 24 hours in air followed by 12-24 hours in a vacuum oven at 120 °C. Electrodes with an area of 1.8 cm^2 were punched from the cast electrode and typically had loadings of about 6-10 mg active material/cm^2 with electrode thicknesses between 150-200 μm. Composite electrodes were assembled into 2032 coin cells with lithium anodes (half cell configurations) and Celgard 3401 separators in a helium filled glove box, using a 1M $LiPF_6$ in 1:2 ethylene carbonate/dimethylcarbonate (EC/DMC) electrolyte solution (Ferro) Alternatively, full cells with $Li_4Ti_5O_{12}$ anodes and $LiFePO_4$ cathodes were assembled in the same configuration.

Battery testing was carried out at room temperature using an Arbin BT/HSP-2043 cycler. $LiFePO_4$ half-cells were charged (delithiated) at a current density equivalent to a constant C/25 rate (assuming a theoretical capacity of 170 mAh/g) and then subjected twice to current discharges at C/25, C/5, C/2, C, 2C, 3C, and 5C rates. $Li_4Ti_5O_{12}$ half-cells were studied for rate capability in both discharge and charge mode: cells were discharged (lithiated) at constant C/25 rate (assuming a theoretical capacity of 175 mAh/g) and then subjected twice to current charges at C/25, C/5, 5C, and 10 C rates, and

vice-versa. $LiFePO_4/Li_4Ti_5O_{12}$ full-cells were cycled at charge/discharge rate of C/25, C/5, C, 5C, and 10C rates. Charges and discharges were carried out between 2.0 - 3.9 V for $LiFePO_4$ half-cells, between 1.0 - 2.5 V for $Li_4Ti_5O_{12}$ half-cells, and between 0.5 – 2.9 V or 0.3-2.9V (for high currents) for $LiFePO_4/Li_4Ti_5O_{12}$ full-cells with 15 min rest between half cycles. Multiple cells were tested to ensure reproducibility. Some cells were subjected to extended constant current cycling either before or after the rate studies.

Results

Physical Characterization

The XRD pattern of $LiFePO_4$ after heat-treatment is shown in Figure 1. The peaks could be indexed to the olivine structure (space group Pnma) and Rietveld analysis showed that the samples are > 98 wt% phase purity with lattice volumes of 291.2±0.1 $Å^3$. Specific surface area values range between 12-30 m^2/g and the carbon content is between 2-4 wt.%. In spite of the high surface area and presence of carbon, the particles have high tap densities of 1.2-1.6 g/cm^3 and pellet densities of 1.7-2.0 g/cm^3. This can be attributed to the uniform, loosely sintered, spherical 50-100 nm particles formed during the pyrolysis process, as shown in Figure 2. High resolution images reveal a 2-4 nm thin coating on the surface of particles with a structure different than the crystalline core. The layered surface coating has a structure similar to turbostratic carbon with the basal planes of graphene layers curved along the particle surface; moreover, the coating appears to be uniform and continuous on the nanoparticle surface. In comparison, other polymeric-precursors typically result in thicker, non-uniform, amorphous coatings and may not be as effective for coating nanosized particles for the same carbon content and tap density.[12-15] The Raman spectrum of a $LiFePO_4$ sample, as shown in Figure 3, is dominated by bands

characteristic of disordered carbons, most prominently the G (graphene) peak near 1590 cm^{-1} and the D (disordered) band at 1350 cm^{-1}, which is correlated with the breakage of symmetry at the edges of graphene sheets. As Raman spectroscopy is surface sensitive, the weak intensity of $LiFePO_4$ peaks (953 cm^{-1}, 997 cm^{-1} and 1098 cm^{-1}) confirm that the carbon is primarily on the surface of the particles. The similarities of the five different spectra, taken at different spots in the sample indicate that the carbon coating is highly uniform on the surfaces of the particles.

The XRD pattern of a typical sample of $Li_4Ti_5O_{12}$ after heat-treatment is shown in Figure 4. The phase composition consists of ~87 wt% $Li_4Ti_5O_{12}$ (Fd-3m, a = 8.362±0.002 Å) and ~13 wt% Li_2TiO_3 (Fd-3m, a = 8.292±0.002 Å). Cubic-Li_2TiO_3 is a high temperature polymorph in the Li_2O-TiO_2 system, quenched to room temperature during the pyrolysis step.[16] The particles have a specific surface area of 10 m^2/g. TEM micrographs of $Li_4Ti_5O_{12}$ are shown in Figure 5; the sample is composed of loosely sintered, faceted 50-200 nm particles. The particles have a tap density of 0.8 g/cm^3 and a pellet density of 1.7 g/cm^3.

Electrochemical Characterization

Typical discharge curves as a function of current density for a Li/carbon-coated nano-$LiFePO_4$ half-cell (Powder A: 27 m^2/g (equivalent sphere = 63 nm), 2.9 wt% C) are shown in Figure 6. No adjustments in specific capacity are made to compensate for the weight of the carbon. The profile at low discharge rates consists of a flat domain at 3.4 V, corresponding to the two-phase reaction $LiFePO_4 \leftrightarrow FePO_4 + Li^+ + e^-$. Specific capacities achieved during early cycles were 150, 147, 138, and 117 mAh/g at C/25, C, 5C, and 10C rates, respectively. Stable performance was observed for 70 cycles, with

retention of 99% and 92% of C/25 discharge-capacity at C and 5C, respectively, as shown in Figure 7.

A graphical summary of results for several of the $LiFePO_4$ samples is given in Figure 8, in the form of a modified Peukert plot, where capacity is plotted vs. C-rate. The rate performance of five other $LiFePO_4$ powders is also included. Powder B is a nanostructured powder (13 m^2/g, 127nm) without carbon-coating; however, 1.6 wt% loose carbon is present from the pyrolysis step, rather than from carbon-coating on the surface of the particles. Powder C (15 m^2/g, 111 nm) is also a nanostructured powder but has a broad particle size distribution and 2.6 wt. % carbon coating. Powder D (6 m^2/g, 278 nm) is a powder using the same starting powder as Powder A; however, minimal amount of organic precursor was used to ensure high phase purity resulting in 0.6 wt% carbon coating. All four powders have greater than 98 wt.% phase purity and lattice volume of 291.2±0.1 $Å^3$.

The organic precursor provides two functionalities in the synthesis process: firstly, a minimal amount of organic precursor is required to avoid impurity phases during firing (including $Li_3Fe_2(PO_4)_3$, Li_3PO_4, and Fe_3O_4) and secondly, the organic precursor controls the excessive particle size growth on heat-treatment (as in the case of Powder D which has minimal amount to ensure high phase purity, albeit resulted in four times larger particle size compared to Powder A). However, the minimal amount of organic precursor used in Powder D is not expected to result in a uniform carbon-coating. Powder B is different in that respect to Powders A, C, and D as it is a high surface area and high phase purity powder without a carbon-coating (and without the use of organic precursor). Powder B was synthesized by modifying the pyrolysis recipe to incorporate carbon in the

nanoparticles which aided in the heat-treatment step. Thus, the carbon in Powder B is rather in a loose form in comparison to a carbon-coating in Powders A, C, and D.

Powders E and F are comparison samples. Powder E is a conventional carbon-coated submicron powder, while Powder F (15 m^2/g, 111 nm) is the state of the art material with 2.3 wt% carbon coating.

Powder D with the largest particle size and lowest carbon content, among the samples in the current study, showed the worst rate performance with <80 mAh/g at all C-rates as shown in Figure 8. Powder B showed good rate-performance owing to its nanostructured particle size distribution, albeit with a lower discharge capacity in comparison to Powders A and C. At lower rates, Powders A and C showed similar performance; however at higher rates, the performance of Powder C was limited because of its larger particle size and broader particle size distribution. It is not clear why the discharge capacity of Powder B is lower, but it does suggest that a polymeric precursor is essential not only to provide good uniform carbon-coating but also in terms of ensuring good phase purity. As expected, conventional submicron Powder E showed poor rate-performance. On the other hand, state of the art Powder F showed good discharge capacity and rate performance; however above 3C, the discharge capacity was lower in comparison to Powder A. For example at 5C, Powder A and F showed discharge capacity of 138 and 133 mAh/g, respectively. Additionally, Powder A developed in this work showed higher tap density of 1.24 g/cm^3, in spite of higher surface area, in comparison to 0.85 g/cm^3 of state of the art Powder F. Tap density is well correlated to the density that can be achieved in coated electrodes and nanostructured particles with carbon content negatively impact the tap density and the practical cell gravimetric and

volumetric energy densities.[15] Therefore, the carbon-coated nanostructured $LiFePO_4$ powder with high tap density developed in this work is better suited for both power and energy applications.

Although the powder were handled and stored in ambient conditions, no evidence of air oxidation was observed for Powders A, B, C, and D in the electrochemical experiments, as described by Martin et al.[17]; i.e. the first charge capacity was found to be larger than the first discharge capacity in this study. On the other hand upon extended cycling, the discharge capacity of Powder C, with submicron sized particles, increases by 10-15% and cell impedances decrease (i.e., lower overpotentials are observed). This may be due either to changes in the particle sizes or improved wetting of the carbon coatings by the electrolytic solution (through, e.g., development of porosity). Comparable improvements upon cycling were not observed for Powders A and B, indicating that the larger $LiFePO_4$ particles behave differently. The test results show that particle size, size distribution, and carbon coating influences the rate capability of $LiFePO_4$; the best result was observed for the carbon-coated, smallest sized particles. In this respect, the organic precursor for carbon-coating serves three purposes: ensures homogenous carbothermal reduction to avoid impurity phases with Fe^{3+} valence state, prevents excessive particle size growth, and ensures an intimately connected conductive coating to promote rapid electron transfer during cycling.

Typical discharge/charge curves for Li/nano-$Li_4Ti_5O_{12}$ half-cell are shown in Figures 9 and 10. The curves show a flat operating voltage at 1.55 V, indicative of the two-phase reaction, $Li_4Ti_5O_{12} + 3Li^+ + 3e^- \leftrightarrow Li_7Ti_5O_{12}$. In spite of the presence of an impurity Li_2TiO_3 phase, the specific capacity achieved was 146 and 148 mAh/g at C/25

discharge and charge rates, respectively. The average operating potential shifts at higher rates due to associated overpotentials, which were much higher in magnitude for the discharge curve, suggesting that Li insertion is slower than lithium extraction. When keeping the discharge rate constant at C/25 and increasing the charge rate, the capacity retention was 93% (138 mAh/g) and 85% (125 mAh/g) of the C/25 charge capacity at 5C and 10C, respectively. In contrast, keeping the charge rate constant and increasing the discharge rate results in a much lower discharge capacity retention of 48% (70 mAh/g) and 22% (32 mAh/g) of C/25 discharge capacity at 5C and 10C, respectively. To determine the effect of voltage limits and cycling history, one fresh cell was tested with a reduced voltage limits between 1.2-2.2 V and another fresh cell was cycled at different discharge rates *de novo*; however no difference was observed on the marked discrepancy between charge and discharge rate behavior.

In a recent study, lithiation and delithiation kinetics of $Li_4Ti_5O_{12}$ has been studied using single particle microvoltammograms and the difference explained based on a two phase (spinel and rock-salt) core-shell model.[18] It was suggested that the lithiation of $Li_4Ti_5O_{12}$ spinel core is limited by lithium diffusion in the electronically conductive $Li_7Ti_5O_{12}$ rock-salt shell, while the delithiation of $Li_7Ti_5O_{12}$ rock-salt core is limited by charge transfer in the low electronically conductive $Li_4Ti_5O_{12}$ spinel shell. The slow lithiation kinetics observed in this study can be partly attributed to the broad particle size distribution (10 m^2/g, 50-200 nm) and resultant longer lithium diffusion path in bigger particles. The presence of impurity Li_2TiO_3 phase is also undesirable as it could not only result in lower capacity but also impede lithium and electronic conduction paths in the electrode. Both particle size and impurity content are related to the heat-treatment

temperature as higher temperatures get rid of impurity phases but result in larger particle size distribution and hence, a compromise is expected to give the best performance. It is interesting in this regard to note that $Li_4Ti_5O_{12}$ with impurity anatase-TiO_2, rutile-TiO_2, and Li_2TiO_3 phases with particle size less than 69 nm has been proposed as an fast lithiation material.[19] Phase pure $Li_4Ti_5O_{12}$ was synthesized on heat-treatment at higher temperatures albeit with five times larger particle size and hence, was not evaluated for electrochemical performance.

Charge and discharge curves of $LiFePO_4/Li_4Ti_5O_{12}$ full cell, where the electrode capacities were matched, are shown in Figure 11. The profiles consist of plateaus at about 1.85 V, as both electrodes undergo two-phase reactions for lithium insertion/extraction. Specific capacities achieved at C/5 charge and discharge rates were 153 and 150 mAh/g (based on the mass of the $Li_4Ti_5O_{12}$ in the negative electrode), respectively. The cell showed good rate capability with 145, 122, and 63 mAh/g at C, 5C, and 10C rates, respectively, when charging and discharging current densities were held the same and voltage limits changed to 0.3-3.2 V for 5C and 10C-rates. At higher rates, the capacity achieved is lower as the overpotentials increase and voltage limits are reached sooner. For example, at the 5C rate, the difference between the discharge and charge curve is about 1 V, which limits the attainable capacity. The large overpotential is due to the comparatively poor rate capability of $Li_4Ti_5O_{12}$ in particular during charge (lithiation), as observed in the $Li_4Ti_5O_{12}$ half cells, as well as impedances associated with the hardware of the coin cells and other components.

The performance of $LiFePO_4/Li_4Ti_5O_{12}$ full cells is very stable over 200 cycles even at 5C and 10C rates, as shown in Figure 12. Slight fading was observed, which was

in general recoverable after charge or discharge current densities was lowered or when voltage limits were modified. This "reversible" capacity fading indicated that no active materials was lost or disconnected but rather the internal impedance of the cell increased gradually to hit voltage limits before the full capacity can be utilized. At 5C, only 0.003% of the capacity is lost per cycle; this can be attributed to the excellent cyclability and chemical stability of both nano-$LiFePO_4$ and nano-$Li_4Ti_5O_{12}$ compositions within the operating voltage range. These results suggest that the low-cost, safe, and non-toxic $LiFePO_4/Li_4Ti_5O_{12}$ cell is a viable system both for 1.5 V consumer electronics and for high-rate applications such as hybrid electric vehicles.[20-23] For both applications, the production of high quality, nanoscale $LiFePO_4$ and $Li_4Ti_5O_{12}$ compositions allow the benefits of excellent rate capability and cyclability to be achieved.

Conclusion

An aerosol pyrolysis method has been used to synthesize nano-$LiFePO_4$ and $Li_4Ti_5O_{12}$ compositions, along with a proprietary method to coat $LiFePO_4$ nanoparticles with a uniform, 2-4 nm thick carbon layer having a structure similar to turbostratic carbon. The $LiFePO_4$ powder show high tap density and pellet density, in spite of the very small particle size and carbon content. In half cells against Li-metal, both nano-$LiFePO_4$ and $Li_4Ti_5O_{12}$ show high rate capabilities. However, the discharge (lithiation) of nano-$Li_4Ti_5O_{12}$ is comparatively slower, which can be explained on a basis of a core-shell model. A tighter particle size distribution and improvements in the phase purity are expected to result in higher discharge rate capabilities of $Li_4Ti_5O_{12}$. $LiFePO_4/Li_4Ti_5O_{12}$ full-cells showed very good rate capabilities with charge/discharge capacity values of 150

and 122 mAh/g at C/5 and 5C, respectively. The cycling performance is especially promising with capacity loss rates of 0.003%/cycle at 5C rate over 200 cycles.

Acknowledgment

Authors are thankful to the management of NanoGram Corp. for their support of this work. Authors would also like to acknowledge Dr. Robert Kostecki for helpful discussions and providing Raman spectra on samples.

This work was also supported by the U.S. Department of Energy under Contract No. DE-AC02-05CH11231.

References

[1] A. K. Padhi, K. S. Nanjundaswamy, and J. B. Goodenough, , *J. Electrochem. Soc.*, **144**, 1188 (1997).

[2] A. Yamada, S. C. Chung, and K. Hinokuma, , *J. Electrochem. Soc.*, **148**, A224 (2001).

[3] D. Peramunage and K. M. Abraham, , *J. Electrochem. Soc.*, **145**, 2609 (1998).

[4] L. Kavan and M. Gratzel, *Electrochemical and Solid State Letters,* **5**, A39 (2002).

[5] P. P. Prosini, M. Carewska, S. Scaccia, P. Wisniewski, S. Passerini, and M. Pasquali, *J. Electrochem. Soc.,* **149**, A886 (2002).

[6] S.-Y. Chung, J. T. Blocking, and Y.-M. Chiang, *Nat. Mater.,* **1**, 123 (2002).

[7] Y. Hu, M. M. Doeff, R. Kostecki, and R. Finones, , *J. Electrochem. Soc.*, **151**, A1279 (2004).

[8] C. H. Chen, J. T. Vaughey, A. N. Jansen, D. W. Dees, A. J. Kahaian, T. Goacher, and M. M. Thackeray, *J. Electrochem. Soc.,* **148**, A102 (2001).

[9] L. Kavan, J. Prochazka, T. M. Spitler, M. Kalbac, M. Zukalova, T. Drezen, and M. Gratzel, *J. Electrochem. Soc.,* **150**, A1000 (2003).

[10] A. Guerfi, S. Sevigny, M. Lagace, P. Hovington, K. Kinoshita, and K. Zaghib, *Journal of Power Sources*, **119-121**, 88 (2003).

[11] J. D. Wilcox, M. M. Doeff, M. Marcinek, and R. Kostecki, *J. Electrochem. Soc.,* **154**, A389 (2007).

[12] K. Zaghib, A. Mauger, F. Gendron, and C. M. Julien, *Solid State Ionics*, **179**, 16 (2008).

[13] S. Myung, S. Komaba, N. Hirosaki, H. Yashiro, and N. Kumagai, *Electrochimica Acta*, **49**, 4213 (2004).

[14] K.Hsu, S. Tsay, and B. Hwang, *J. Mater. Chem.*, **14**, 2690 (2004).

[15] Z. Chen and J. R. Dahn, *J. Electrochem. Soc.,* **149**, A1184 (2002).

[16] H. Kleykamp, *Fusion Engineering and Design*, **61-62**, 361 (2002).

[17] J. F. Martin, A. Yamada, G. Kobayashi, S. Nishimuta, R. Kanno, D. Guyomard, and N. Dupre, *Electrochemical and Solid State Letters,* **11**, A12 (2008).

[18] N. Takami, H. Inagaki, T. Kishi, Y. Harada, Y. Fujita, and K. Hoshina, *J. Electrochem. Soc.,* **156**, A128 (2009).

[19] H. Inagaki and N. Takami, *US Patent Application* 2006/0257746.

[20] L. Persi, F. Croce, and B. Scrosati, *Electrochemistry Communications*, **4**, 92 (2005).

[21] S. Franger, C. Bourbon, and F. Le Cras, *J. Electrochem. Soc.,* **151**, A1024 (2004).

[22] J. Dahn, J. Jiang, L. Moshurchak, C. Buhrmester, and R. L. Wang, *The Electrochemical Society Interface*, Winter 2005, 27

[23] X. Hu, Y. Huai, Z. Lin, J. Suo, and Z. Deng, *J. Electrochem. Soc.,* **154**, A1026 (2007).

Figure Captions

1) XRD powder pattern of nano-$LiFePO_4$ using Cr-Kα radiation.

2) TEM micrographs of nano-$LiFePO_4$.

3) Raman spectra of carbon coated nano-$LiFePO_4$; spectra taken at five different spots. The D (disordered) and G (graphene) bands of carbon are marked, as is a peak attributable to $LiFePO_4$ (LFP).

4) XRD powder pattern of nano-$Li_4Ti_5O_{12}$ using Cu-Kα radiation.

5) TEM micrograph of nano-$Li_4Ti_5O_{12}$.

6) Discharge curves at different C-rates for a Li/nano-$LiFePO_4$ half-cell (Powder-A: 27 m^2/g, 2.9 wt% carbon-coating).

7) Cycling performance of a Li/nano-$LiFePO_4$ half-cell (Powder-A: 27 m^2/g, 2.9 wt% C).

8) Rate performance of lithium half-cells containing several different $LiFePO_4$ materials Powder-A: 27 m^2/g, 2.9 wt% carbon-coating; Powder-B: 13 m^2/g, 1.6 wt% loose carbon; Powder-C: 15 m^2/g (broad particle size distribution), 2.6 wt% carbon-coating, Powder-D: 6 m^2/g, 0.6 wt% carbon-coating, Powder-E: conventional carbon-coated submicron powder, Powder-F: state of the art powder, 15 m^2/g, 2.3 wt% carbon-coating.

9) Discharge/charge curves at different charge (delithiation)-rates for Li/nano-$Li_4Ti_5O_{12}$ half-cell; all discharges at C/25 rate.

10) Discharge/charge curves at different discharge (lithiation)-rates for Li/nano-$Li_4Ti_5O_{12}$ half-cell; all charges at C/25 rate.

11) Discharge/charge curves for a $LiFePO_4$/$Li_4Ti_5O_{12}$ full-cell at several different rates.

12) Cycling performance of a $LiFePO_4$/$Li_4Ti_5O_{12}$ coin full-cell.

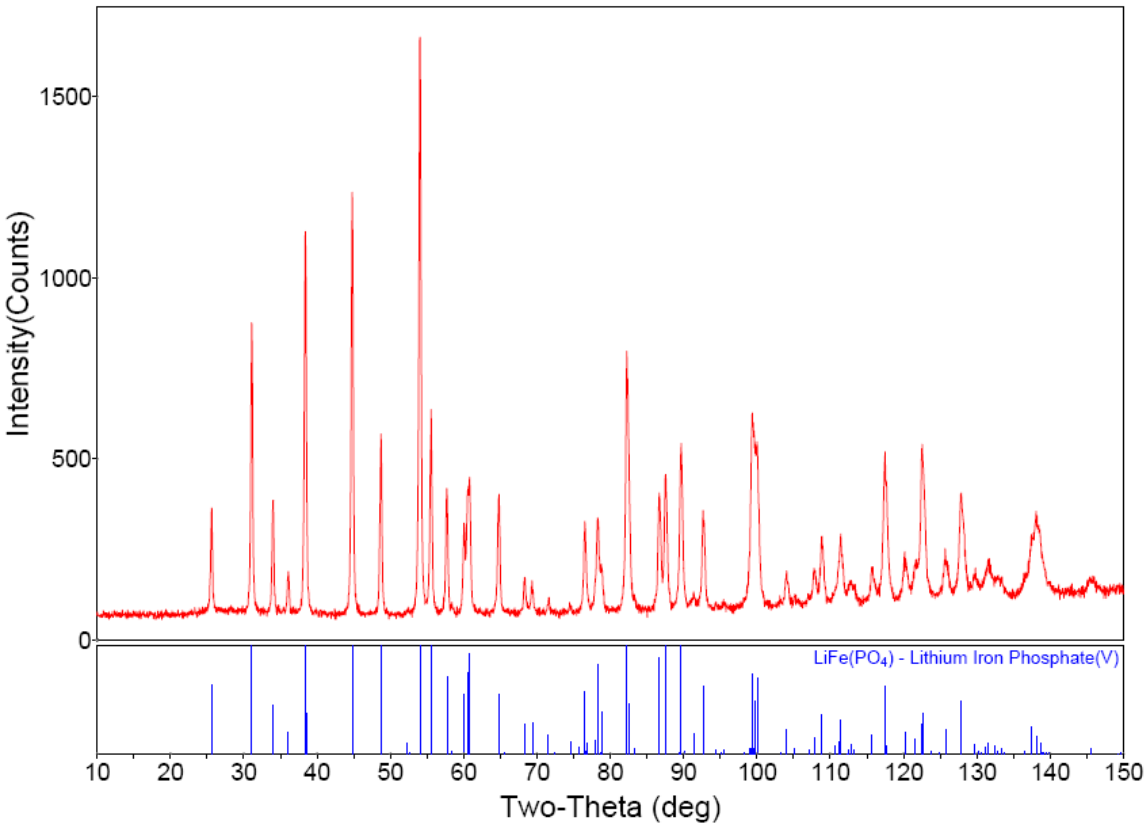
Intensity(Counts)
1500
1000
500
0
LiFe(PO4) - Lithium Iron Phosphate(V)
10
20
30
40
50
60
70
80
90
100
110
120
130
140
150
Two-Theta (deg)

Figure 1.

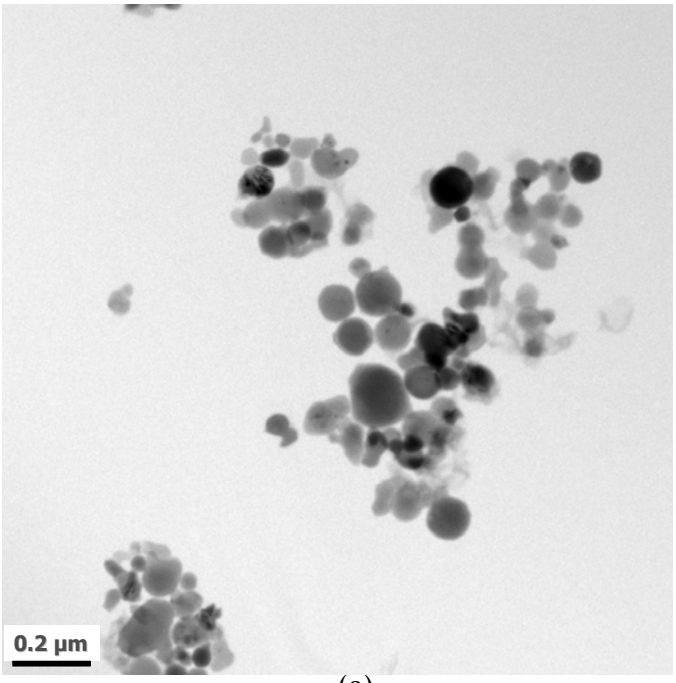

(a)

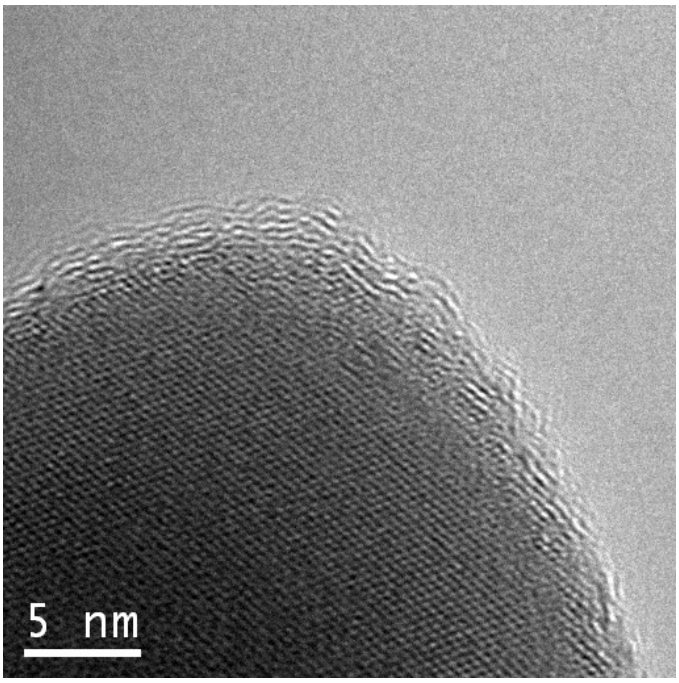

(b)

Figure 2.

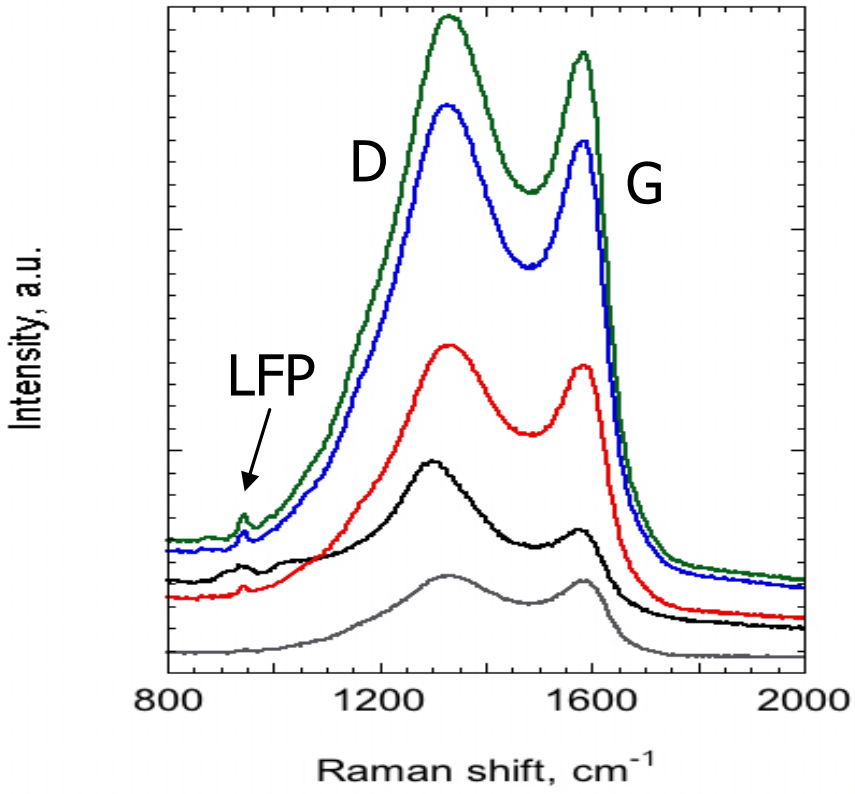

Figure 3.

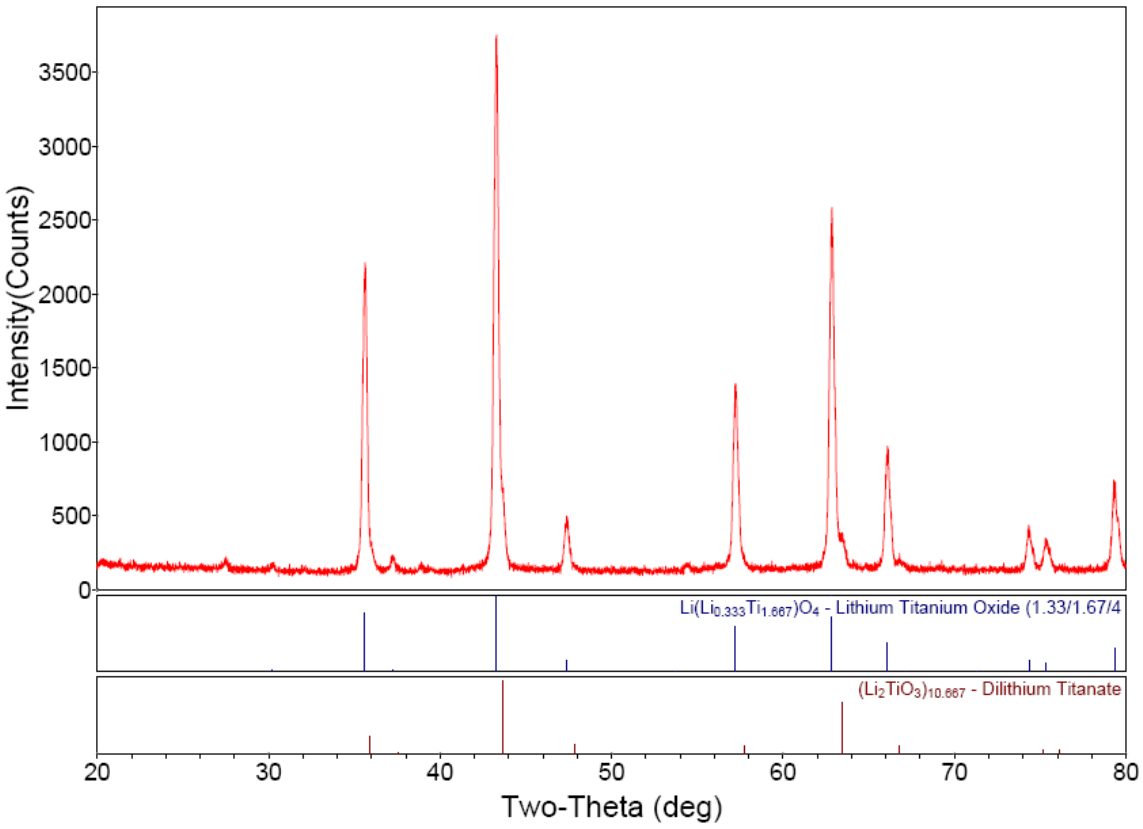
Intensity(Counts)
3500
3000
2500
2000
1500
1000
500
0
Li(Li0.333Ti1.667)O4 - Lithium Titanium Oxide (1.33/1.67/4
(Li2TiO3)10.667 - Dilithium Titanate
20
30
40
50
60
70
80
Two-Theta (deg)

Figure 4.

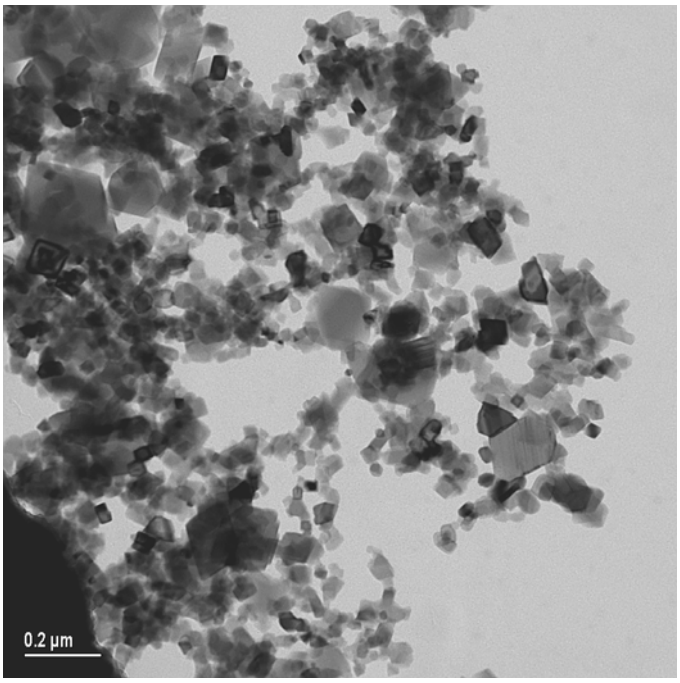

Figure 5.

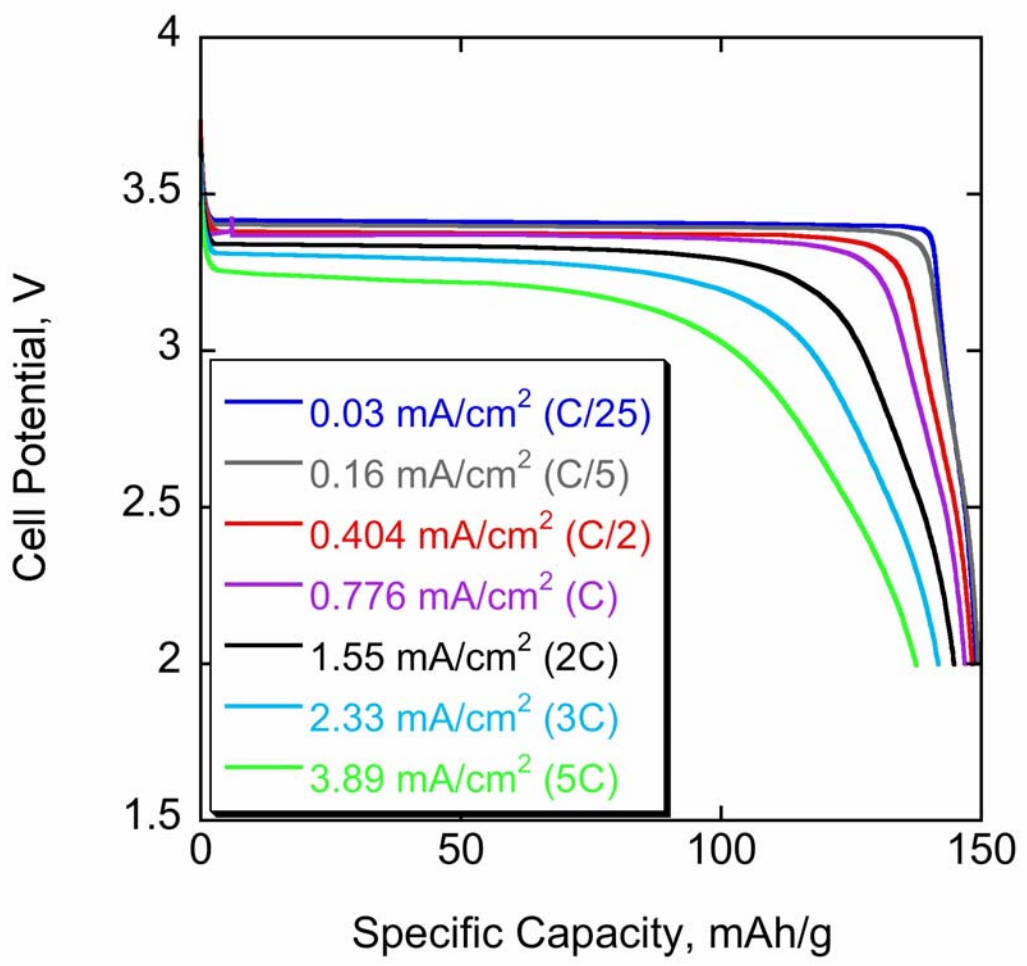
Cell Potential, V
Specific Capacity, mAh/g
4
3.5
3
2.5
2
1.5
0
50
100
150
0.03 mA/cm2 (C/25)
0.16 mA/cm2 (C/5)
0.404 mA/cm2 (C/2)
0.776 mA/cm2 (C)
1.55 mA/cm2 (2C)
2.33 mA/cm2 (3C)
3.89 mA/cm2 (5C)

Figure 6.

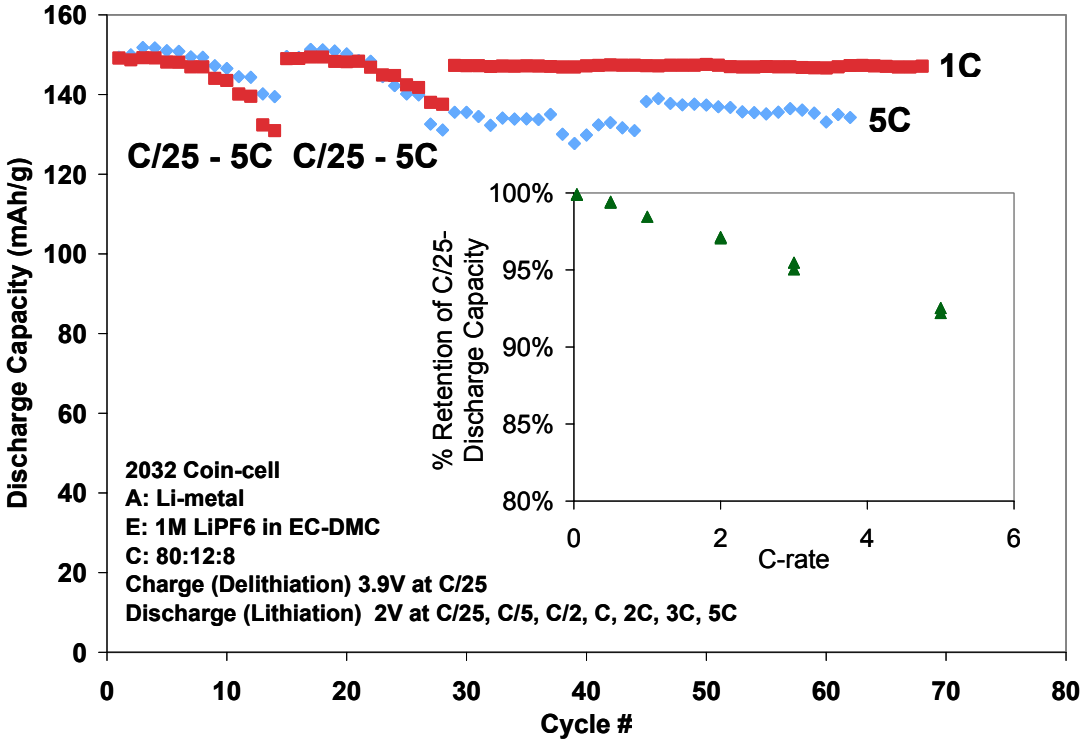
Discharge Capacity (mAh/g)
Cycle #
1C
5C
C/25 - 5C C/25 - 5C
2032 Coin-cell
A: Li-metal
E: 1M LiPF6 in EC-DMC
C: 80:12:8
Charge (Delithiation) 3.9V at C/25
Discharge (Lithiation) 2V at C/25, C/5, C/2, C, 2C, 3C, 5C
% Retention of C/25-Discharge Capacity
C-rate

Figure 7.

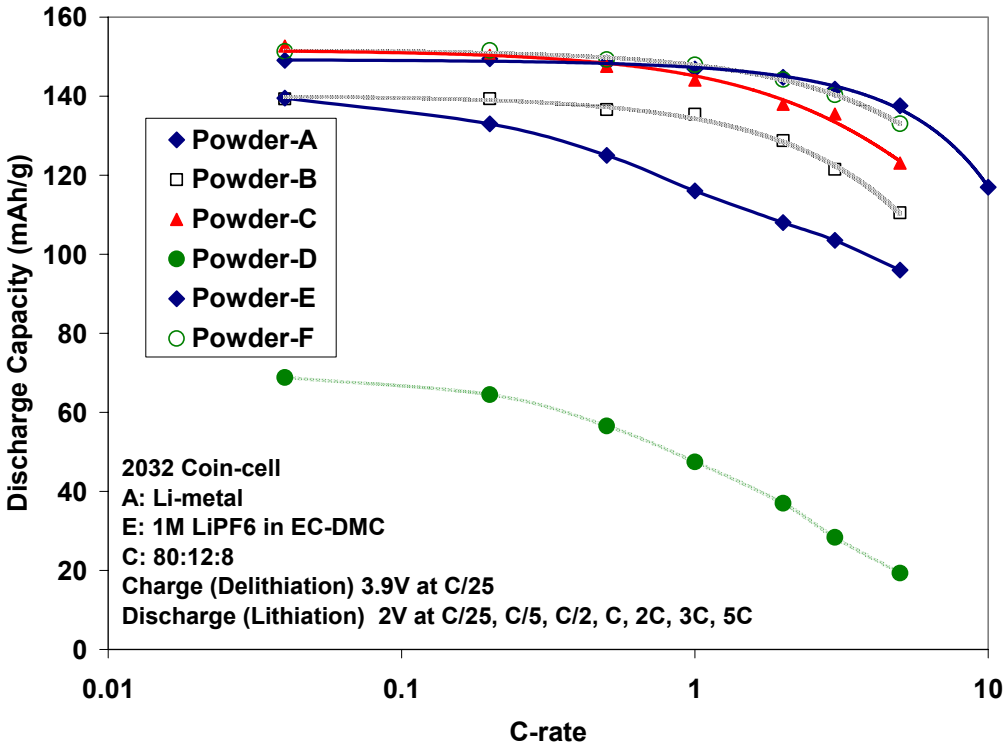
Discharge Capacity (mAh/g)
C-rate
160
140
120
100
80
60
40
20
0
0.01
0.1
1
10
Powder-A
Powder-B
Powder-C
Powder-D
Powder-E
Powder-F
2032 Coin-cell
A: Li-metal
E: 1M LiPF6 in EC-DMC
C: 80:12:8
Charge (Delithiation) 3.9V at C/25
Discharge (Lithiation) 2V at C/25, C/5, C/2, C, 2C, 3C, 5C

Figure 8.

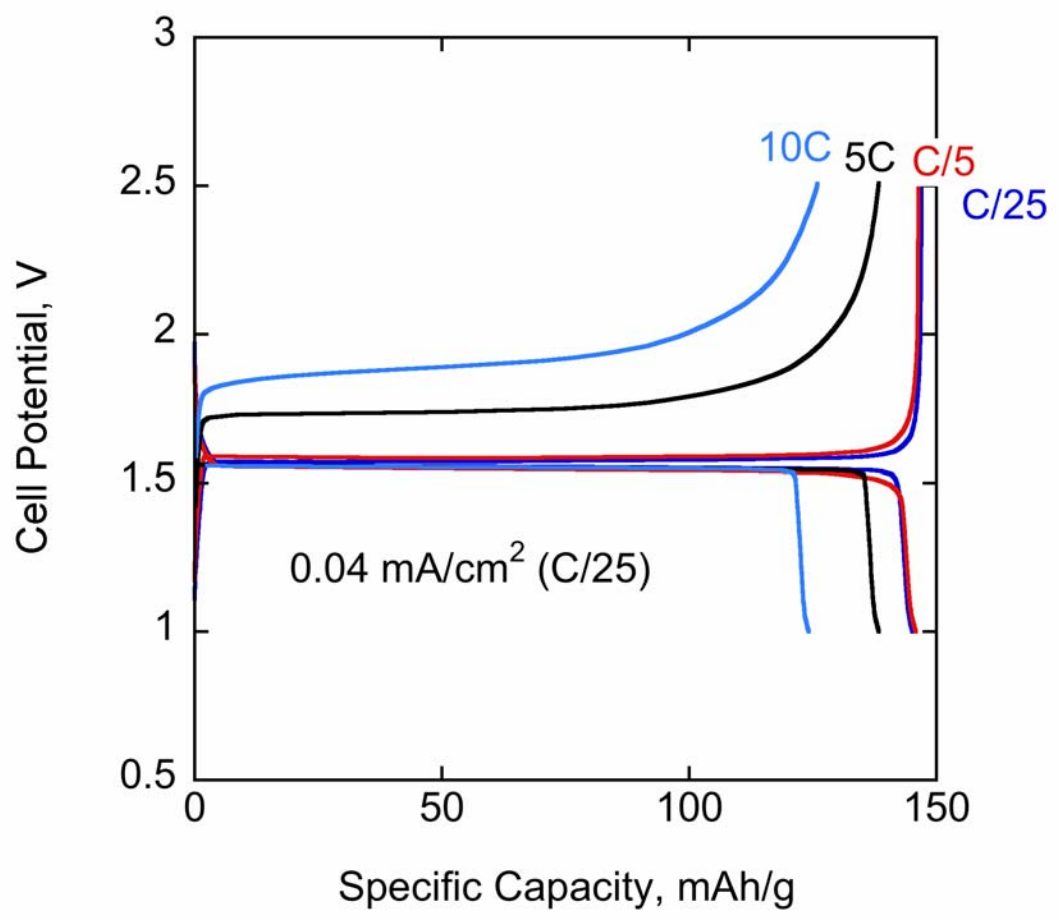
3
2.5
2
1.5
1
0.5
0
50
100
150
Cell Potential, V
Specific Capacity, mAh/g
10C
5C
C/5
C/25
0.04 mA/cm2 (C/25)

Figure 9.

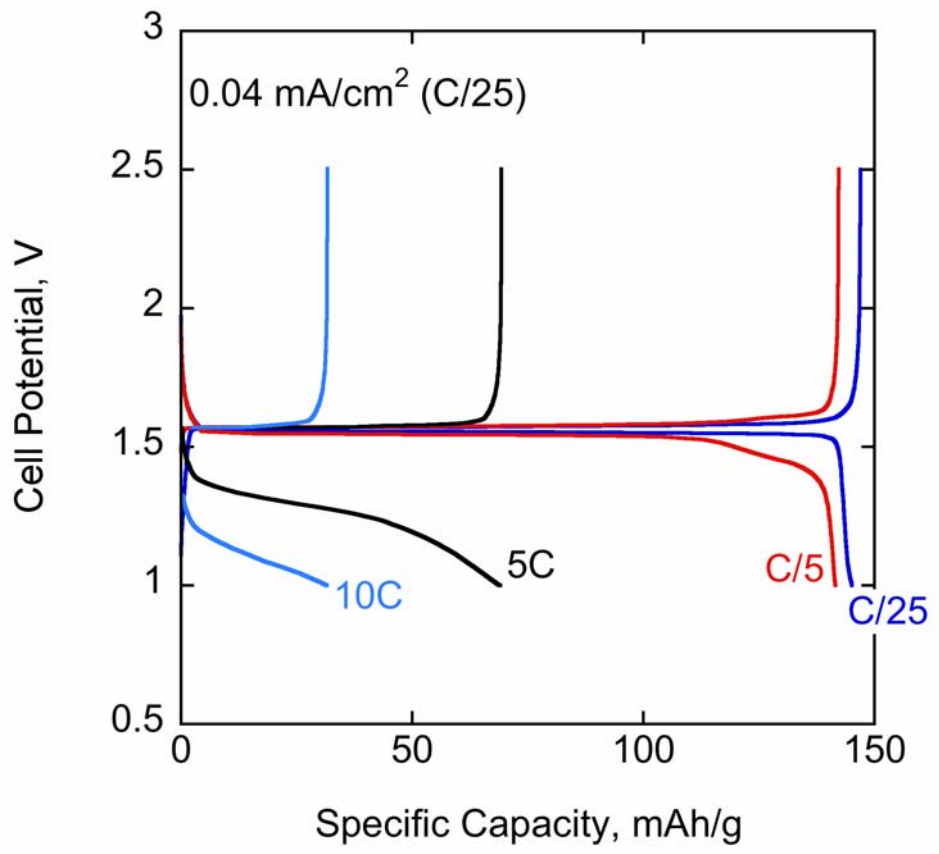
0.04 mA/cm2 (C/25)
Cell Potential, V
Specific Capacity, mAh/g
10C
5C
C/5
C/25
3
2.5
2
1.5
1
0.5
0
50
100
150

Figure 10.

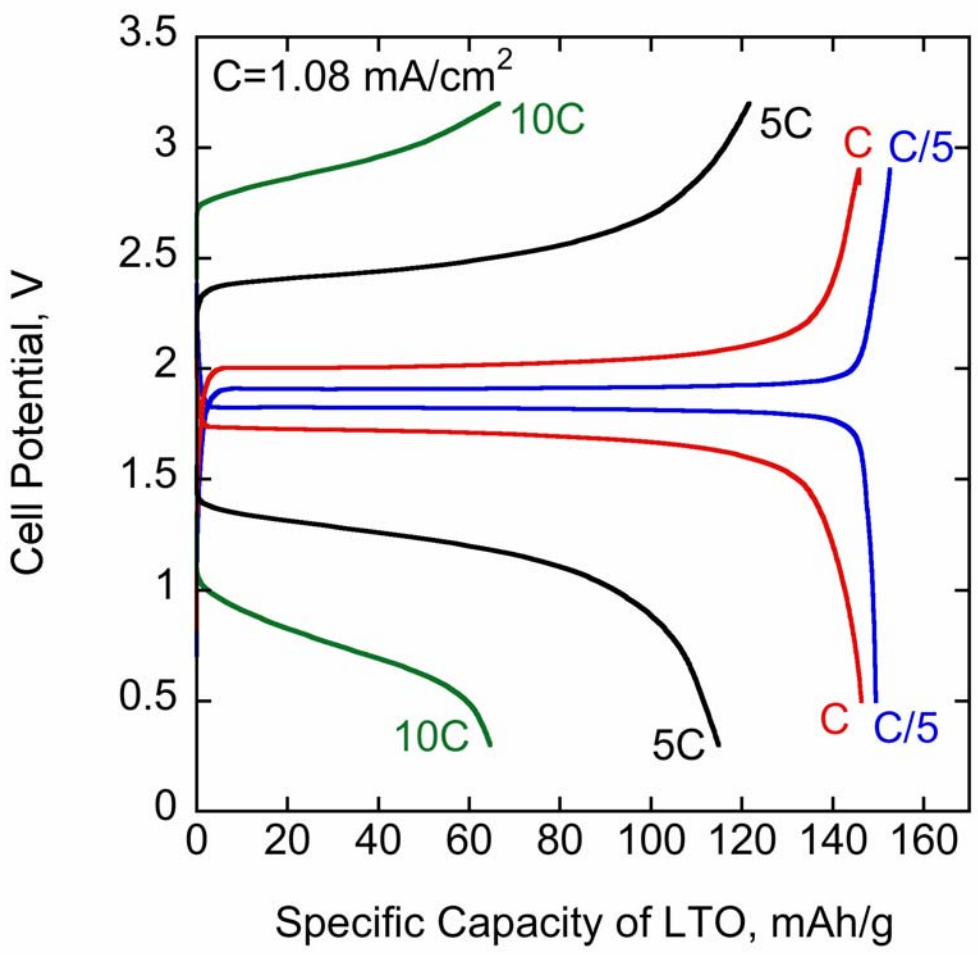
C=1.08 mA/cm2
10C
5C
C
C/5
10C
5C
C
C/5
Cell Potential, V
Specific Capacity of LTO, mAh/g
0
0.5
1
1.5
2
2.5
3
3.5
0
20
40
60
80
100
120
140
160

Figure 11.

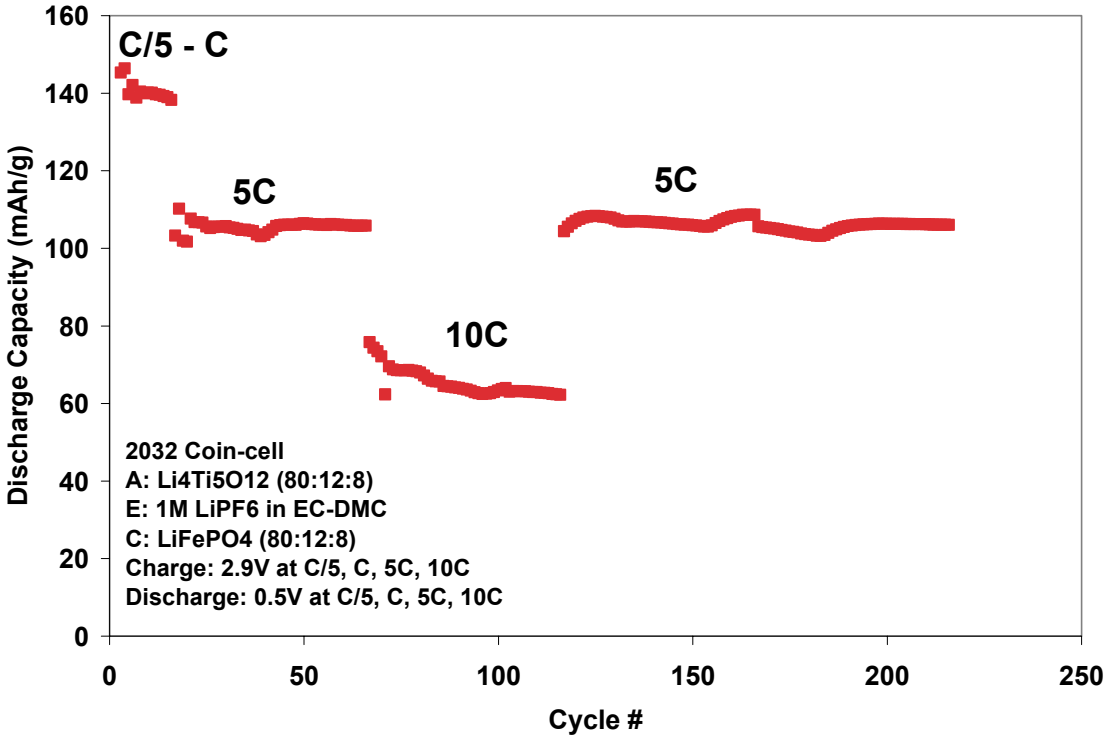
C/5 - C
5C
5C
10C
2032 Coin-cell
A: Li4Ti5O12 (80:12:8)
E: 1M LiPF6 in EC-DMC
C: LiFePO4 (80:12:8)
Charge: 2.9V at C/5, C, 5C, 10C
Discharge: 0.5V at C/5, C, 5C, 10C
Discharge Capacity (mAh/g)
Cycle #
0
20
40
60
80
100
120
140
160
0
50
100
150
200
250

Figure 12.